Interaction between tunnel excavations and historical structures in Rome: a fully coupled structural and geotechnical approach

Angelo Amorosi[1,*], Sebastiano Rampello[1], Marialuigia Sangirardi[2] and Giorgio Mattucci[3]

[1] Department of Structural and Geotechnical Engineering, Università di Roma La Sapienza
Via Eudossiana 18, 00184, Roma (Italy)
angelo.amorosi@uniroma1.it

[2] Department of Engineering Science, University of Oxford
Parks Road, OX1 3PL, Oxford, UK

[3]Civil engineer, Roma (Italy)

Abstract In this paper we propose a 3D Finite Element (FE) approach to model the excavation of twin tunnels, accounting for the strongly non-linear soil behaviour, interacting with monumental masonry structures, carefully modelling their geometry and non-linear anisotropic mechanical behaviour. The work focuses on a specific case-study related to the ongoing construction of the line C of Rome underground.

Keywords: Tunnel construction, Masonry, Soil-Structure interaction, Nonlinearity

1 Introduction

Development of urban mobility in densely populated cities implies the construction of tunnels often interacting with valuable historical structures. It is thus necessary to develop rational and reliable procedures to estimate the potential damage induced by tunnelling. This corresponds to solve the related soil-structure interaction problem. Classical approaches can be used to this purpose that, however, adopt relatively simple schemes for either one or both components of the problem, such as springs for the soil or equivalent plates for the structure. These simplifying assumptions prove to be appropriate for conventional soil-foundation interaction problems, while show some limitations when tackling more complex problems, as those involving the excavation in proximity or beneath heavy and stiff historical masonry structures. In these circumstances, the need for a reliable prediction of the damage induced by tunnelling on historical structures justifies the adoption of more advanced numerical approaches, based on realistic constitutive hypotheses for both the soils and the masonries, together with an accurate modelling of the excavation process. This is what proposed in this paper, where a 3D FE approach is adopted to model the tunnel excavation, the strongly non-linear soil behaviour and the non-linear anisotropic response of masonry structures, the latter here

included accounting for their 3D geometry. This contribution focuses on a specific case-study related to the ongoing construction of the line C of Rome underground.

2 Case study

The line C of Rome underground runs from South-East to North-West of the city, with a total length of 25.6 km. It is characterised by twin tunnels with a single track, excavated using an earth pressure balance (EPB) tunnel boring machine (TBM) with an outer diameter D = 6.7 m, at depths of 27 to 55m and average distances of 20 to 40m.
Contract T3 of the line, which runs for 3.6 km between the *Amba Aradam/Ipponio* and the *Fori Imperiali/Colosseo* stations is currently under construction. This paper focuses on the portion of the line which under-passes the ancient *Aurelian walls* at *Porta Metronia*, about 250 m West of the *Amba Aradam/Ipponio* station (Fig. 1).

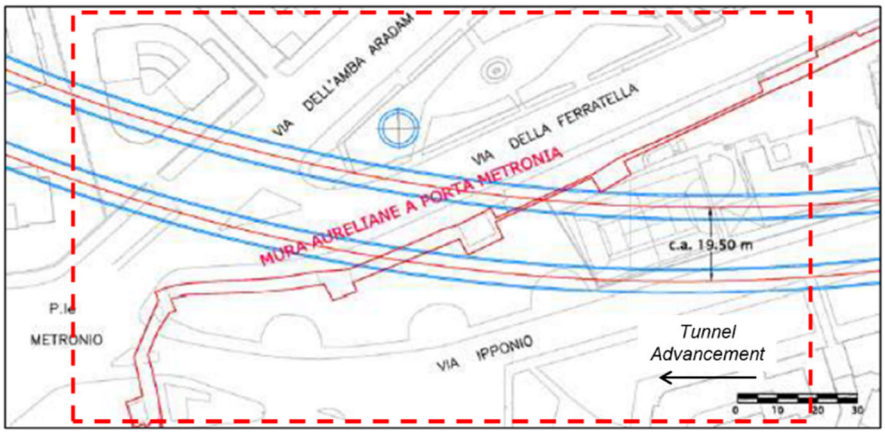

Fig. 1 Plan view of the model (dashed red line).

The odd and even tunnels under-cross the *Aurelian Walls* at depths of 27.5m and 28m, respectively, with a cover to tunnel diameter ratio C/D = 3.60 and 3.68: both tunnels form an angle of about 30° with the wall axis, in plan, and deepen below the wall with a slope of about 3%.
The ground conditions at the site are shown in Fig. 2, which refers to the longitudinal section through the odd tunnel. It is characterised by an upper layer of coarse-grained made ground (MG), about 13 m thick, overlying the alluvial deposits of Pleistocene age. These consist of a layer of sandy silt and silty sand (LSO), underlain by a layer of sandy gravel (SG). A thick deposit of stiff and overconsolidated clay from the Pliocene is found underneath the gravel, at about 3m below the sea level. The profile of hydraulic head shows a downward seepage in the silty soil, from the made ground towards the gravel, between 16 and 2 m a.s.l. (Fig. 3).

The *Aurelian Walls* are large defensive walls built by Emperor Aurelian between 270 and 275 A.C. Most of their length (12.5 km over 19 km) has survived past centuries in a fairly good preservation state. *Porta Metronia* is in the Southeastern part of the town wall. Both in-situ and laboratory tests have been performed to detect masonry characteristics and identify its mechanical properties.

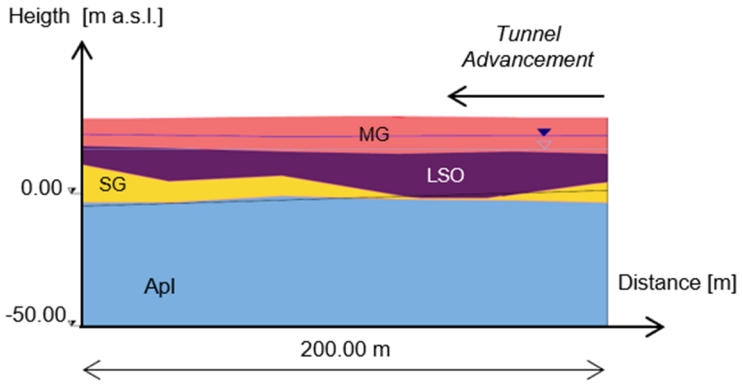

Fig. 2 Detail of the ground stratigraphy along the odd tunnel.

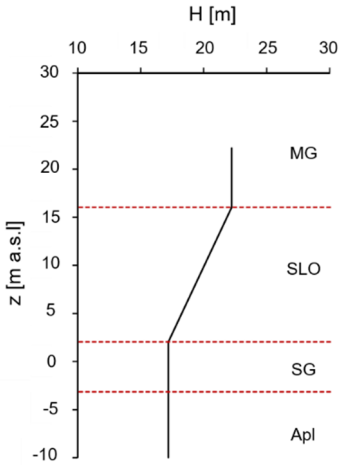

Fig. 3 Assumed profile of the hydraulic head.

The geometry of the wall section has been determined through endoscopic surveys, while stiffness and strength properties were evaluated via ultrasonic tests, flat-jacks and compressive tests on mortar and core drill specimens. The analysed portion of the walls is characterised by a complex geometry that has been evaluated referring to five different branches (Fig. 4). The first branch (*b6-b7*) is made by a single leaf structure, 2.3 m high and 1 m thick; the second one (*b7-b8*), similar to the former, is characterised by the presence of defensive towers 9 m high, of 5.2×9 m^2 in plan; the third branch (*b8-b9*) ends with another tower of 8.3×10.15 m^2 in plan, and a total height of 12 m. In the *b9-*

b10 branch, the original configuration of the walls is clearly visible, with the two facings connected by a series of arches and barrel vaults. The last section (*b10-b11*) is characterised by the presence of another tower, followed by a double facing portion of the walls very similar to the previous one.

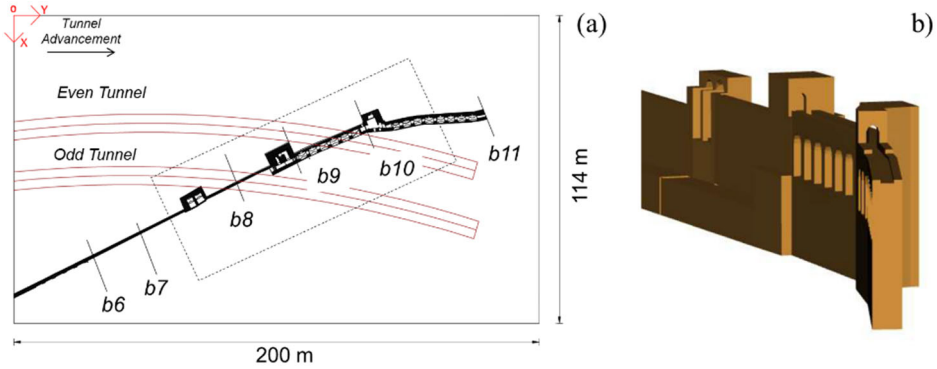

Fig. 4 Plan identification of *Walls* sections (a) and 3D view of the structural model (dashed box) (b).

3 Numerical modelling and results

The numerical study was performed by the FE code Plaxis 3D. The model was set up to simulate the twin tunnel excavation under free-field conditions and in presence of the *Aurelian Walls*. Vertical boundaries of the model were restrained horizontally, normal to the mesh sides, while the base of the mesh was restrained both horizontally and vertically. The analysis was performed as follows: model initialisation; walls construction (only in the coupled analysis); odd tunnel excavation; even tunnel excavation. The excavation of each tunnel is simulated by a step-by-step procedure consisting of a series of progressive advancements, each having the length of one concrete lining ring according to the procedure reported in Fargnoli *et al*. (2015).

All the analyses here discussed were carried out before the actual construction of the infrastructure, imposing the design volume loss $V_L = 0.5$ % and neglecting the activation of possible mitigation measures to prevent tunnelling-induced damage, such as compensation grouting, included in the final design. The soil profile was described according to the in-situ one (Fig. 2) for both the free-field and the interaction model. The mechanical behaviour of the soils was described using the Hardening Soil model with small-strain stiffness (*HSsmall*, Benz, 2007) for the sandy silt and the Hardening soil model (*HS*, Schanz *et al*., 1999) for the other layers. All the model parameters, summarised in Table 1, were calibrated based on the extensive geotechnical investigation, consisting of several in situ and laboratory tests, discussed in detail in Rampello *et al*. (2019).

The constitutive model adopted for masonry is a three-dimensional anisotropic elastic-perfectly plastic one (Lasciarrea *et al*., 2019), in which block aspect ratio and staggering joints effects are considered.

Table 1 Soil model parameters.

Soil	Model	γ kN/m^3	c' kPa	φ' °	G_0^{ref} MPa	$\gamma_{0.7}$ %	ν'	$E'_{ur}{}^{ref}$ MPa	$E'_{50}{}^{ref}$ MPa	$E'_{oed}{}^{ref}$ MPa	m
MG	*HS*	17	5	34	-	-	0.2	240	24	24	1
LSO	*HSsmall*	19.5	28	27	125	0.04	0.2	150	8.2	5.52	0.8
SG	*HS*	20	0.1	40	-	-	0.2	900	90	90	0.4
Apl	*HS*	20.9	41.3	25.7	-	-	0.2	960	48	48	1

Macroscopic elastic properties are derived in the framework of homogenisation theory of periodic media, while yielding is characterized by the intrinsic material anisotropy. A set of (maximum) three sliding directions, on which failure is meant to occur, is defined in the *xyz* space and described by means of dip and strike angles, representing, for each plane, the positive rotation along the *x*-axis and the negative rotation along the *z*-axis, respectively (Amorosi and Sangirardi, 2021). In the analyses only two planes (head and bed joints) are activated. Yield functions are defined, for each orientation, in terms of local stress components according to Coulomb's and tensile criterion as follows:

$$f_i^c = \tau_i + \sigma_{n,i} \tan\phi_i - c_i \tag{1}$$

$$f_t^i = \sigma_{n,i} - \sigma_{t,i} \tag{2}$$

where i = 1,2,3 stands for the plane, $\sigma_{n,i}$ and τ_i are the normal and the shear stress along each orientation, ϕ_i is the friction angle, c_i is the cohesion and $\sigma_{t,i}$ is the tensile strength along the joints. The interlocking effect is accounted by modifying the strength parameters on the head-joints plane, stemming from equilibrium conditions and considering the aspect ratio of the blocks through the parameter β, which depends on the friction angle of the bed joints:

$$\beta = \tan\phi_2 \frac{b}{2a} \tag{3}$$

Tensile strength and cohesion on the head joints are hence calculated according to the following expressions:

$$\sigma_{t,1} = \sigma_{t0,1} - \beta\sigma_{n,2} + c_{0,2}\frac{\beta}{\tan\phi_2} \tag{4}$$

$$c_1 = c_{0,1} - \left(\beta\sigma_{n,2} - c_{0,2}\frac{\beta}{\tan\phi_2}\right)\tan\phi_1 \cdot \tag{5}$$

The constitutive parameters adopted in the analysis are summarized in Table 2.

Table 2 JMM constitutive parameters.

G	ν	γ	ϕ	$c_{0,i}$	$\sigma_{t0,i}$	β
MPa	-	kN/m^3	°	kPa	kPa	-
1000	0.15	10	30	50	25	1.8

A free field (FF) analysis was first performed, comparing the numerical results with available semi-empirical estimates of ground settlements (in which $K = 0.4$). Fig. 5 refers to the section sketched in the right bottom corner. The subsidence curves are computed at the foundations level of the wall (19.0 m a.s.l.): the comparisons refer to settlement troughs as obtained at the end of the excavation of the odd tunnel (black lines) and at the end of the even tunnel (red lines).

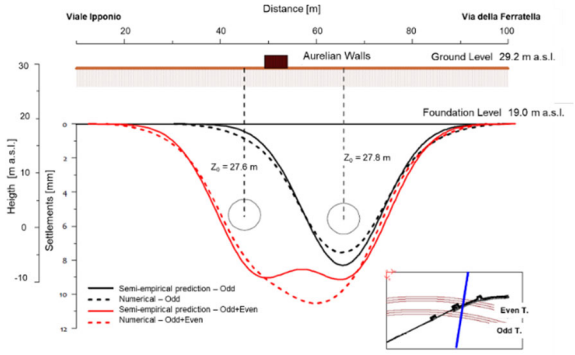

Fig. 5 Settlement troughs at the walls foundation level according to semi-empirical predictions and numerical results (free-field conditions).

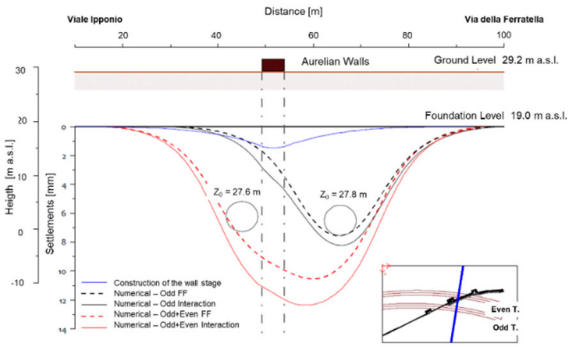

Fig. 6 Settlement troughs at the walls foundation level according to semi-empirical predictions and numerical results (interaction conditions, displacement set to zero after wall construction phase).

For the first single odd tunnel, the numerical and semi-empirical predictions are in reasonable agreement; instead, they exhibit different patterns when referring to the excavation of both tunnels, because of the plasticity-related non-linear interaction effects,

realistically accounted for by the numerical model but disregarded in the empirical approach. Fig. 6 compares the above free field analysis results with those obtained by the coupled analysis, in which the 3D tunnel excavations are simulated considering the presence of the *Aurelian Walls*. It reports the subsidence profile at the same location considered in the FF case, at the end of each of the stages defined in the previous paragraph. The interaction with the surface structure leads to larger settlements, while substantially preserving the shape of the settlement troughs, apart from their portions directly corresponding to the structure, where the stiffness of this latter results in a lower inflection of the curves. A top view of the magnified deformed mesh of the walls allows to understand the kinematic developing during the entire process. Fig. 7 shows the trace of the undeformed walls and the deformed one at the end of the excavation of the first tunnel (a) and of both tunnels (b), highlighting the out-of-plane rotation induced by tunnelling.

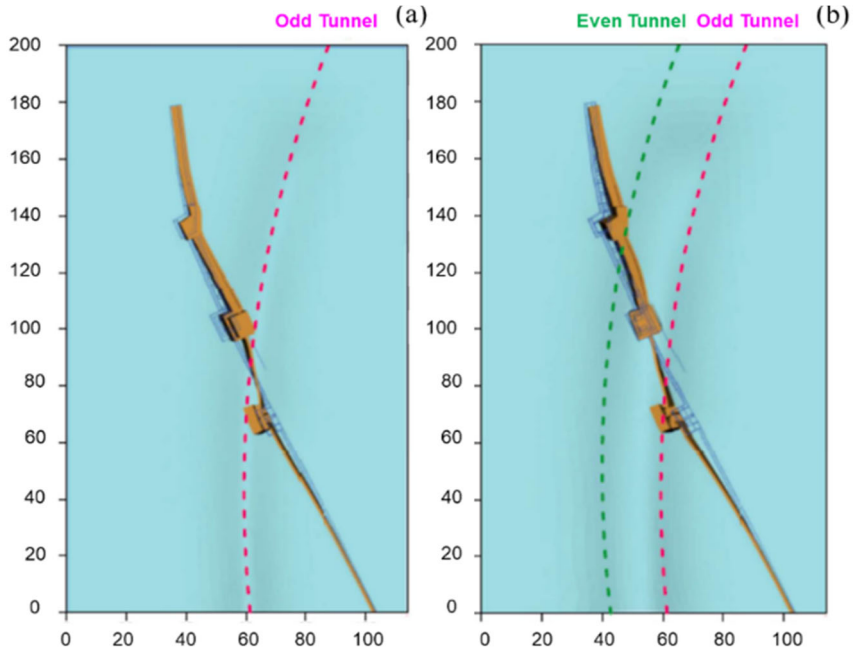

Fig. 7 Magnified deformed mesh at the end of the excavation of the odd (a) and even tunnel (b).

Evident torsional effects characterize the response of the structure during the excavation process, resulting in the tensile strain patterns illustrated in Fig. 8, traditionally adopted to interpret damage intensity and distribution (Boscardin and Cording, 1989). The same figure also plots the evolution of plastic points as observed within the structure during the construction stages, showing that the greater development of plastic strains is computed during excavation of the even tunnel (phase 110), when they concentrate at the wall-towers connection. It can be concluded that in the case under study the worse damage conditions do not necessarily correspond to the final stage, when the excavation of both tunnels is completed.

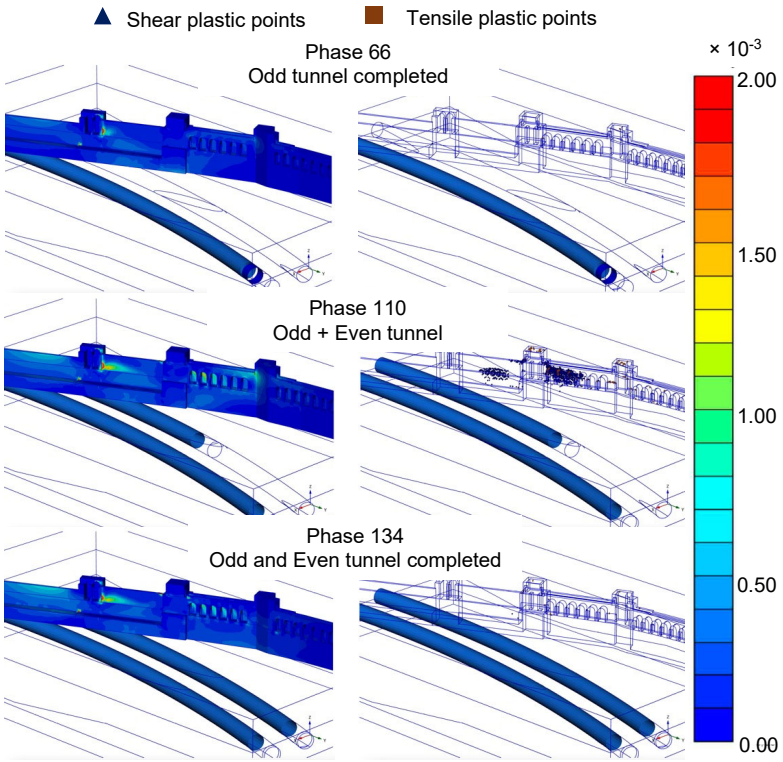

Fig. 8 Tensile strain and plastic point distribution at different stages of the excavations.

References

Amorosi, A. and Sangirardi, M. (2021). Coupled three-dimensional analysis of the progressive tunnelling-induced damage to masonry buildings: is it always worth it?. *Tunnelling and Underground Space Technology*, *118*, 104173.

Benz, T., 2007. *Small-strain stiffness of soils and its numerical consequences*. Ph.D. thesis, Universität Stuttgart.

Boscardin, M. D., and Cording, E. J. (1989). Building response to excavation-induced settlement. *Journal of Geotechnical Engineering*, 115(1), 1-21.

Fargnoli, V., Gragnano, C. G., Boldini, D., & Amorosi, A. (2015). 3D numerical modelling of soil–structure interaction during EPB tunnelling. *Géotechnique*, *65*(1), 23-37.

Lasciarrea, W.G., Amorosi, A., Boldini, D., de Felice, G. and Malena, M. (2019). Jointed Masonry Model: A constitutive law for 3D soil-structure interaction analysis. *Engineering Structures*, 201, 109803.

Rampello S., Fantera L. and Masini L. (2019). Efficiency of embedded barriers to mitigate tunnelling effects. Tunnelling and Underground Space Technology, 89, 109-124.

Schanz, T., Vermeer, P.A. and Bonnier. P. G. (1999). The hardening soil model: formulation and verification. *Beyond 2000 in computational geotechnics*, 281-296.